MODERN ASTRONOMY:
FROM THE EARLY UNIVERSE TO EXOPLANETS AND BLACK HOLES

Multipoint multiwavelength observations of a near-the-limb eruptive solar flare with quasi-periodic pulsations

I. Zimovets and I. Sharykin

Space Research Institute of the Russian Academy of Sciences, 84/32, Profsoyuznaya St, Moscow, 117997 Russia

Abstract. We present results of the analysis of multiwavelength observations of the M3.4 eruptive flare that occurred near the western limb of the Sun on September 2, 2023 (SOL2023-09-02T06:33). We use observations from the near-Earth spacecraft ASO-S/HXI, SDO/AIA, HMI, GOES/XRS, and Fermi/GBM. X-ray observations by the STIX telescope-spectrometer on board the Solar Orbiter from the opposite side of the Sun are also used. The flare was associated with a two-stage inclined ($\approx 40-50^\circ$ to the radial direction) eruption, the second stage of which was accompanied by the impulsive flare phase and quasi-periodic pulsations (QPPs) of hard X-rays with a characteristic time scale $P \approx 1.56$ min. HXI observed hard X-ray sources located above the apex of a coronal Y-shaped structure, visible in the "hot" 94 and 131 Å EUV channels, behind a drop-shaped erupting plasmoid/prominence. Hard X-ray sources near the foot of the flare loops and flare ribbons were also observed, mainly after the peak of the impulsive phase. The HXI and STIX observations from different locations in the heliosphere are consistent with each other. Temporal dynamics of the spectral index of nonthermal electron flux had a "soft-hard-soft" behavior during QPPs. The observational results do not contradict the "standard" model of eruptive two-ribbon flares, where populations of electrons are accelerated episodically due to magnetic reconnection in a current sheet in the corona behind an erupting structure. However, understanding the quasi-periodicity of electron acceleration/injection requires further studies.

Keywords: Sun: flares; X-rays, gamma rays; UV radiation; coronal mass ejections (CMEs)

DOI: 10.26119/VAK2024.125

1 Introduction

Solar flares are a phenomenon of rapid transformation of magnetic energy of active regions (ARs) into other types of energy, e.g., kinetic energy of accelerated particles and their electromagnetic emission. Many flares are accompanied by quasi-periodic pulsations (QPPs). Despite large number of proposed mechanisms, there is still no complete understanding of processes leading to QPPs (e.g., Kupriyanova et al. 2020; Zimovets et al. 2021). In this regard, further detailed multi-wavelength observations with spatial resolution of QPP sources are of considerable interest. In particular, it is important to perform an analysis of observations of flares near the solar limb, for which we can determine vertical spatial structure of pulsation sources and study their relationship with eruptive processes. This may be useful for refining the "standard model" of two-ribbon flares and for incorporating the QPP mechanisms into this model.

The aim of this work is to present the results of a preliminary analysis of the M3.4-class eruptive solar flare that occurred on September 2, 2023 near the western edge of the solar disk (N06W89) in the NOAA AR 13413 of β and Dkc classes.

2 Observational data

The flare was observed by a number of space-based instruments. In the X-ray range, the flare was observed by the Hard X-ray Imager (HXI) (Zhang et al. 2019) onboard the Advanced Space-based Solar Observatory (ASO-S) (Gan et al. 2019) and by the Gamma-ray Burst Monitor (GBM; Meegan et al. 2009) onboard the Fermi in the low-Earth orbits, as well as by the X-Ray Sensor on the Geostationary Operational Environmental Satellite (GOES-16). The flare X-ray emission was also detected from the opposite side of the Sun by the Spectrometer/Telescope for Imaging X-rays (STIX; Krucker et al. 2020) onboard the Solar Orbiter (SolO). SolO was at a distance of 0.681568 AU from the Sun, the angle between the Earth, Sun's center and SolO was 155.678°, and thus the angle between the flare site, Sun's center and SolO was $\approx 66.7°$ (see Fig. 2(i)). Additionally, we used observations in the UV and EUV channels of the Atmospheric Imaging Assembly (AIA; Lemen et al. 2012) and line-of-sight magnetograms by the Helioseismic and Magnetic Imager (Scherrer et al. 2012) onboard the Solar Dynamics Observatory. Consideration of ground-based observations of the flare is beyond the scope of this article.

3 Observation analysis

Temporal behavior of X-ray emission intensities in different energy ranges is shown in Fig. 1(a–d). The flare was associated with two increases of X-ray emission. The

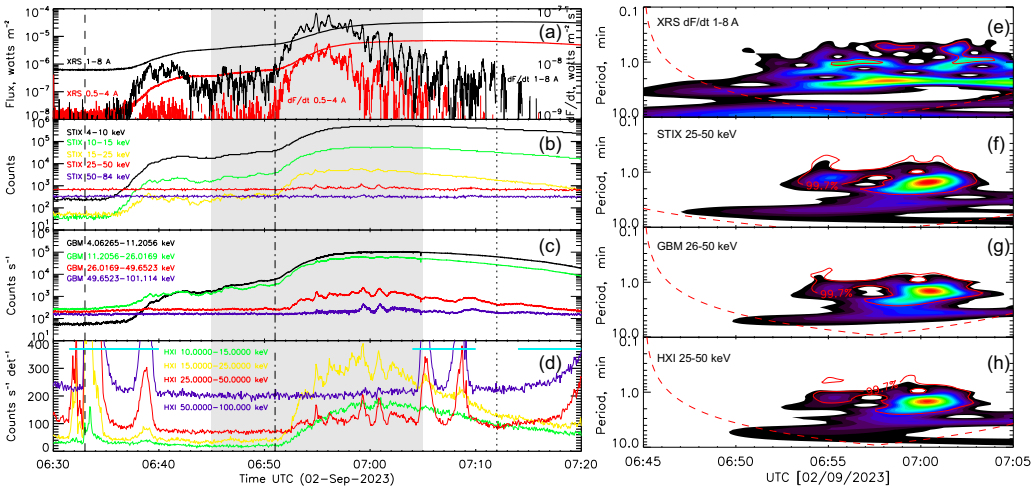

Fig. 1. (Left column) Temporal profiles of X-ray emission detected with different instruments: (a) fluxes in the GOES/XRS channels (thick, left Y-axis) and its derivative (thin, right Y-axis), (b) SolO/STIX, (c) Fermi/GBM, (d) ASO-S/HXI. The vertical dashed, dotted, and dashed-dotted lines indicate the begin, maximum of the flare X-ray flux, and the start of the impulsive phase with QPPs, respectively. The cyan horizontal lines in (d) show intervals when hard X-ray data of HXI was contaminated with radiation belts particles. (Right column) Wavelet spectra of interpolated, detrended, smoothed, and normalized profiles of X-ray emission in the time interval indicated by the gray rectangle in the left column: (e) time derivative of XRS 1–8 Å channel, (f) counts in the STIX 25–50 keV, (g) GBM $\approx 26-50$ keV, (h) HXI 25–50 keV channels.

first less intense one started at 06:33 UT and the second more powerful started at around 06:51 UT. The first increase was associate with a relatively slow rise of coronal structures observed in EUV and the second stage was associated with the fast development of an eruption. The second stage was accompanied with a sequence of hard X-ray ($\approx 15-80$ keV) QPPs (≈06:53–07:03 UT), it was the flare impulsive phase. Wavelet analysis of detrended, normalized and smoothed data of the three instruments (HXI, GBM and STIX) show that these QPPs had a characteristic time scale $P \approx 1.56$ min (Fig. 1(f–g)). These hard X-ray QPPs were not harmonic oscillations. Amplitudes and times between successive peaks were not stable.

At first, the sources of these hard X-ray QPPs were observed in the corona above the bright EUV flare loops seen in 94 and 131 Å (Fig. 2(a, d)), in the region below the departed (at an angle of $40-50°$ to the radial direction) eruptive prominence. Near the middle of the QPP series, in addition to the coronal hard X-ray sources, sources from below began to be observed in the vicinity of the UV flare ribbons (Fig. 2(b, e)). There were signs of a double coronal source in the corona, the centroids at higher energies located slightly above the centroids of the lower-energy sources. After that,

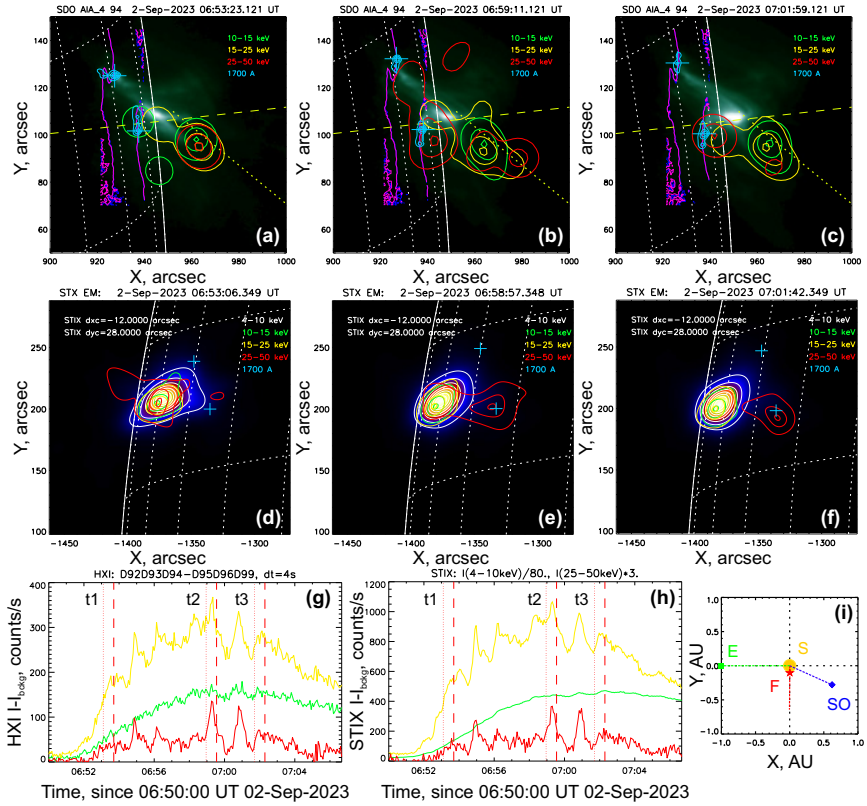

Fig. 2. (a–c) Images of the flare region from near the Earth SDO and ASO-S, and from the SolO/STIX (d–f) for three time intervals $t1 - t3$ indicated in (g, h). The background in (a–c) is the SDO/AIA 94 Å image and in (d–f) is the STIX 4–10 keV image. The cyan contours show the flare ribbons in the AIA 1700 Å, the crosses show positions of its brightest pixels. Hard X-ray sources are shown with the green (10–15 keV), yellow (15–25 keV), and red (25–50 keV) contours at 15, 55, 95% of the maxima. The yellow dashed and dotted straight lines show the radial direction through the flare site and approximate eruption direction, respectively. The blue/red curves show contours of the LOS magnetic field by SDO/HMI at ±5 Gauss. Count rates of HXI and STIX are shown in (g) and (h), respectively. The difference in light travel times from the Sun to Earth and to SolO, $dt = 163$ s, is compensated. (i) The location of the Sun (yellow), Earth (green), SolO (blue), and the flare (red) in the Ecliptic plane.

the coronal hard X-ray sources (> 25 keV) became almost invisible, and only the lower hard X-ray sources were visible (Fig. 2(c, f)) near the flare ribbons. It is worth noting that the HXI and STIX images (at different angles of view of the flare region) are in consistence with each other – they show similar morphology and dynamics of the X-ray sources.

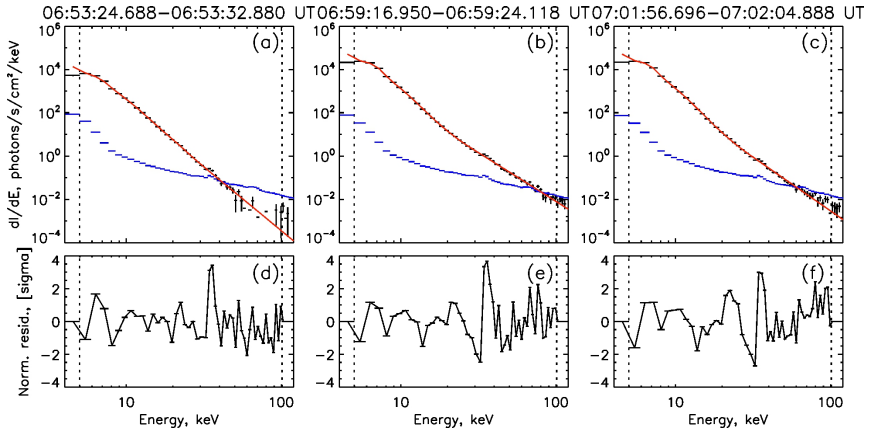

Fig. 3. (a–c) Examples of background-subtracted X-ray spectra (black), their fits with the "thermal" plus "thick2"-target models (red), and the background spectra (blue) made with Fermi/GBM data for three time intervals (see Fig. 4) within three longer intervals in Fig. 2. Errors are shown with vertical bars. (d–f) The corresponding normalized residuals.

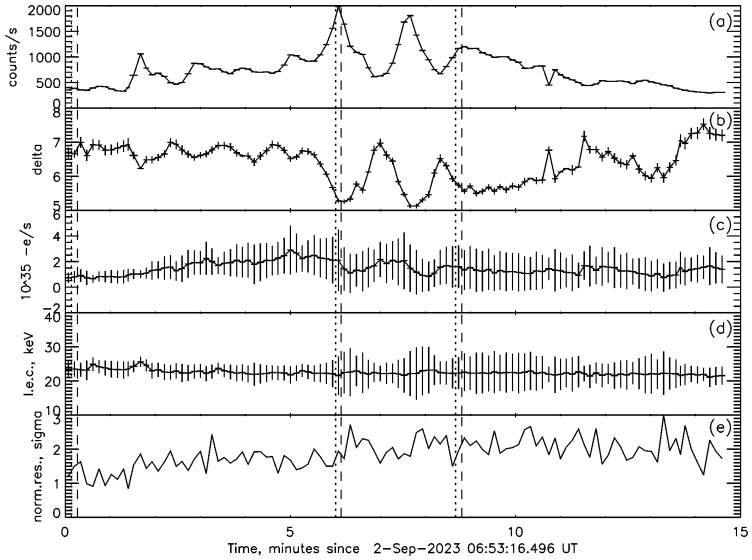

Fig. 4. Temporal profiles of parameters from fitting of X-ray spectra by Fermi/GBM data with the "thermal" plus "thick2"-target models: (a) integrated count rate in $\approx 25-100$ keV, (b) spectral index of electron flux below break, (c) total integrated electron flux, (d) low energy cutoff, (e) normalized residuals. Errors are shown with vertical bars. Pairs of vertical dotted and dashed lines indicate starts and ends of three time intervals for which the spectra are shown in Fig. 3.

We performed spectral analysis of X-ray emission (in $\approx 5-100$ keV range) detected by Fermi/GBM during the impulsive phase. Fitting of the background-

subtracted spectra was done with the use of a combination of two bremsstrahlung models: the "thermal" plasma and "thick2"-target model of nonthermal electrons (with fixed break energy, electron spectral index above the break, and high energy cutoff). Examples of the spectra with the fit model for three time intervals are shown in Fig. 3. Spectra above ≈ 15 keV are mainly the bremsstrahlung spectrum of nonthermal electrons. Dynamics of nonthermal electrons' parameters (spectral index below break, total flux, and the low energy cutoff), intensity of hard X-ray emission in $\approx 25 - 100$ keV and normalized residuals are shown in Fig. 4, from where it is seen that the electron spectral index anticorrelated with the hard X-ray intensity ($cc \approx -0.75$) and presented the "soft-hard-soft" behavior during the QPPs.

4 Conclusions

The analysis of multi-wavelength observations made with different instruments at different locations has shown that the observed QPPs are likely the result of episodic acceleration of electrons in the corona above the flare loops and below the eruptive prominence. It is consistent with the "standard" model of eruptive flares. Understanding the mechanisms underlying the quasi-periodicity requires further research.

Acknowledgements. We are grateful for the usage of ASO-S / HXI, GOES / XRS, Fermi / GBM, SolO / STIX, SDO / AIA, HMI data. SDO is a mission for NASAs Living With a Star (LWS) program. ASO-S mission is supported by the Strategic Priority Research Program on Space Science, the Chinese Academy of Sciences, Grant No. XDA15320000. We thank Prof. W.-Q. Gan for the opportunity to conduct part of this work at PMO CAS, Drs. Yang Su and Zhentong Li for help with the HXI data, and Dr. Tomek Mrozek for imaging the STIX data.

Funding

This work was supported by the Russian Science Foundation grant No. 23-72-30002.

References

Gan W.-Q., Zhu C., Deng Y.-Y., et al., 2019, Research in Astronomy & Astrophysics, 19, 11, id. 156
Kupriyanova E.G., Kolotkov D.Yu., Nakariakov V.M., et al., 2020, Solar-Terrestrial Physics, 6, 1, p. 3
Krucker S., Hurford G.J., Grimm O., et al., 2020, Astronomy & Astrophysics, 642, id. A15
Lemen J.R., Title A.M., Akin D.J., et al., 2012, Solar Physics, 275, 1-2, p. 17
Meegan C., Lichti G., Bhat P.N., et al., 2009, Astrophysical Journal, 702, p. 791
Scherrer P.H., Schou J., Bush R.I., et al., 2012, Solar Physics, 275, 1-2, p. 207
Zimovets I.V., McLaughlin J.A., Srivastava A.K., et al., 2021, Space Science Reviews, 217, 5, id. 66
Zhang Z., Chen D.-Y., Wu J., et al., 2019, Research in Astronomy and Astrophysics, 19, 11, id. 160